Available online at www.sciencedirect.com
SCIENCE DIRECT
Surface & Coatings Technology 200 (2006) 2917–2922
SURFACE & COATINGS TECHNOLOGY
www.elsevier.com/locate/surfcoat

Structural evolution in ZrN_xO_y thin films as a function of temperature

L. Cunha[a,*], F. Vaz[b], C. Moura[a], L. Rebouta[b], P. Carvalho[b], E. Alves[c], A. Cavaleiro[d], Ph. Goudeau[e], J.P. Rivière[e]

[a]Departamento de Física, Universidade do Minho, Campus de Gualtar, Largo do Paco, Braga 4700-320, Portugal
[b]Departamento de Física, Universidade do Minho, Azurém, Guimarães 4800-058, Portugal
[c]Departamento de Física, ITN, E.N.10, Sacavém 2685, Portugal
[d]Faculdade de Ciências e Tecnologia, ICEMS-Universidade de Coimbra, Coimbra 3030, Portugal
[e]Laboratoire de Métallurgie Physique, Université de Poitiers, Futuroscope 86960, France

Received 16 July 2004; accepted in revised form 24 September 2004
Available online 5 November 2004

Abstract

Single-layered zirconium oxynitride (ZrN_xO_y) thin films have been deposited on steel substrates, at a constant temperature of 300 °C, by radiofrequency (rf) reactive magnetron sputtering of a pure Zr target in an argon–oxygen–nitrogen atmosphere. The variation of the flow rate of the reactive gases enabled changes in the composition and structure of the films. X-ray diffraction (XRD) and glancing incidence X-ray diffraction (GIXRD) were used to study the as-deposited films and their structural changes during or after heat treatment, from 400 to 900 °C, in controlled atmosphere and in vacuum.

The as-deposited films revealed the occurrence of a face-centred cubic (fcc) phase (Zr–N type), but a Zr–N oxygen-doped phase (Zr–N–O) may be also present depending on the oxygen content in the films. Heat treatment above 600 °C reveals the appearance of a tetragonal phase of zirconium oxide.

The results are discussed as a function of the chemical composition of the films, annealing temperature, and type of the annealing process.

Keywords: Zirconium oxynitride; PVD coatings; Decorative coatings; Heat treatment

1. Introduction

Transition metal nitride films are used in many applications because of their remarkable mechanical and tribological properties, diffusion behaviour, and chemical inertness [1,2]. In addition, these nitrides may exhibit an interesting, but limited, range of colours (golden yellows, different shades of grey, and black tones) [3,4], allowing them to be used as decorative coatings. Transition metal oxide thin films are used frequently as optical coatings [5]. Recently, a new class of materials has become important for decorative, but poorly explored, oxynitrides: MeN_xO_y (Me=transition metal). Oxygen is more reactive than nitrogen [6] and, due to this higher reactivity, the addition of a small amount of oxygen to a growing transition metal nitride film induces the production of ionic metal–oxygen bonds in a matrix of covalent metal–nitrogen bond. This fact creates a new structure with different properties, and the optical and decorative characteristics of these ceramic materials may be enhanced. The control of the oxide/nitride ratio allows tuning of the band gap, bandwidth, and crystallographic order between oxide and nitride and, in consequence, the electronic properties of materials and their colours.

There has been recent published works about the production and characterization of titanium oxynitrides using chemical vapor deposition (CVD) [7] or physical vapor deposition (PVD) [6,8–12] processes. In a PVD

* Corresponding author. Tel.: +351 53 604066, +351 53 604320; fax: +351 53 678981.
E-mail address: lcunha@fisica.uminho.pt (L. Cunha).

0257-8972/$ - see front matter © 2004 Elsevier B.V. All rights reserved.
doi:10.1016/j.surfcoat.2004.09.030

process with two reactive gases, the control of the correct deposition parameters may be difficult to achieve [8]. To prevent instability phenomena, Martin et al. [6,9] suggest a continuous flow of nitrogen and a pulsed oxygen flow. Chappe et al. [10] used a pulsed water vapour flow instead of oxygen, obtaining, in certain conditions, films with golden-orange metallic colour. The variation of oxygen content in titanium oxynitride film composition [11,12] gave origin to a wide range of colours—richer than the one achieved with the nitrides: from the glossy golden type for low oxygen content (characteristic of TiN films) to dark blue for higher oxygen content. Zirconium oxynitrides have also been produced by DC magnetron sputtering. When the reactive gas in working atmosphere is oxygen, or oxygen-dominant, XRD data show the formation of monoclinic zirconia (m-ZrO_2) crystallites [2], whereas when the reactive gas is nitrogen, the formation of face-centred cubic (fcc) zirconium nitride is detected. Production of zirconium oxynitrides with low oxygen partial pressure, when compared to nitrogen partial pressure, may promote the formation of a new crystalline ZrON phase [13]. In this work, the production of zirconium oxynitride thin films by reactive radiofrequency (RF) magnetron sputtering and the structural, mechanical, and optical characterizations of the produced samples are reported.

PVD-produced ceramic materials are frequently non-stoichiometric and may contain lattice point defects and impurities [1]. In the case of ternary compounds, like oxynitrides, the defects may also be atoms of one of the nonmetallic elements occupying substituting positions in crystalline lattices, or occupying interstitial sites. Heat treatments promote diffusion processes and suppression of defects. Rosa and Hagel [14] report the diffusion of nitrogen in zirconium nitride at the temperature range 700–900 °C. Metal diffusion is much more difficult. The self-diffusion of zirconium in zirconium nitride is registered above 2400 °C [15].

PVD processes induce intrinsic compressive residual stresses in the produced films due to lattice defects, resulting from the growing process itself, where ion bombardment and substrate temperature have a particular role [1]. The residual stresses have a relationship with the hardness of these ceramic materials because they hinder dislocations. Annealing processes may promote lattice defect diffusion and cause stress relaxation. On the other side, the heat, within certain limits, may induce an increase of grain size or give origin to new crystalline phases.

The area of metal oxynitrides is poorly explored, and the understanding of the fundamental mechanism that explains structure, mechanical, optical, and diffusion behaviours is still insufficient. Taking this into consideration, the main purpose of this work consists of the study of the structural evolution of ZrN_xO_y films as a function of composition, temperature, and type of annealing process.

2. Experimental details

ZrN_xO_y films were deposited by RF magnetron sputtering, in rotation mode (4 rpm) from high-purity Zr target, onto mechanically polished stainless steel (AISI 316) substrates. Prior to all depositions, the substrates were ultrasonically cleaned and, in situ, sputter-etched for 10 min in a pure Ar atmosphere (200 W RF power) at 0.4 Pa. The films were deposited in an Ar/N_2+O_2 atmosphere in an Alcatel SCM650 apparatus. The base pressure in the deposition chamber was about 10^{-4} Pa and the working pressure was around 4×10^{-1} Pa. To improve adhesion, a metallic zirconium interlayer, with a thickness of about 0.30 μm, was deposited on each sample. The films were produced with variation of the reactive gas mixture flux (N_2+O_2), under constant temperature (300 °C), RF power (800 W to 2.55 W/cm^2), and substrate bias voltage (−50 V). The reactive gas partial pressure varied from 0.02 to 0.05 Pa. The inert gas (argon) flow rate was kept constant at 100 sccm.

Rutherford backscattering spectrometry (RBS) was used to measure the atomic composition of the samples after deposition, using a 1-MeV $^1H^+$ beam. To characterize the structure of the produced samples, X-ray diffraction (XRD) experiments were performed using a Philips X'pert PW3040 apparatus (Co K_α radiation) in a glancing incidence X-ray diffraction (GIXRD; θ=2°) configuration and a Philips PW 1710 apparatus (Cu K_α radiation) in a conventional $\theta/2\theta$ configuration.

The evolution of the structure as a function of the temperature was studied in two different ways:

i) Controlled atmosphere environment: The GIXRD patterns of each sample were obtained in situ at six temperatures (400–900 °C in 100 °C steps) in a protected Ar/H_2 atmosphere (5.02% of H_2) with a working pressure of 3 Pa, after a base pressure of 0.02 Pa. Two additional XRD patterns were obtained at room temperature, before and after heat treatment.
ii) Vacuum: Each sample suffered five annealing experiments, each one during 1 h, in vacuum (10^{-4} Pa) at five different temperatures (400–800 °C in 100 °C steps). After each one of these annealing experiments, the samples were removed from the furnace and an XRD pattern of each sample was obtained, at room temperature, using the conventional $\theta/2\theta$ configuration.

3. Results and discussion

3.1. Chemical analysis

The composition of the samples was measured by RBS using the RUMP code simulations [16]. The composition is strongly influenced by the reactive gases' partial pressure

during deposition. The composition and thickness of the films are presented on Table 1.

3.2. Structure

The XRD patterns of the analysed samples reveal a strong dependence of the ZrN_xO_y film structure on composition.

The GIXRD pattern of sample ($Zr(NO)_x$) presents three broad peaks, resulting of the overlap of fcc (111) ZrN (JCPDS card 65-2905), hcp (100) and (101) Zr (JCPDS card 5-665), and hcp (100) and (101) α-$ZrN_{0.28}$ (JCPDS card 40-1275) peaks, as may be seen in Fig. 1. The positions of the Zr and α-$ZrN_{0.28}$ peaks are too close to be clearly distinguished. This film was produced with low reactive gas flow rate, where the percentage of oxygen is much lower than the one of nitrogen. The presence of these gases in the reactive atmosphere may cause the insertion of these atoms in the crystalline lattices. The possible interstitial or substituting location of nitrogen (and oxygen) atoms in Zr crystallites and of oxygen atoms in α-$ZrN_{0.28}$ and ZrN crystallites would cause distortion of lattices (stressed states), resulting in broad diffraction peaks corresponding to small crystallites but also to diffraction peak overlaps due to crystals with different lattice parameters (nonhomogeneous stress).

For intermediate values of the flow rate of reactive gases (samples $ZrN_{1.14}O_{.14}$ and $ZrN_{0.95}O_{0.22}$), the GIXRD patterns reveal mainly the occurrence of a ZrN fcc phase (Fig. 1), with the presence of peaks correspondent to diffractions in (111) and (200) planes. Conventional XRD evidences a (200) preferred orientation. Fig. 2 shows de XRD patterns of the samples around the angular position of (200) ZrN peak (the line indicates the position of the unconstrained ZrN).

The increase of the reactive gas flow rates is followed by the appearance of a broad band (around $2\theta=35^\circ$), which may be an indication of either the amorphization of the ZrN phase induced by the oxygen inclusion, or the formation of an amorphous oxide phase. This amorphous phase is related to the increase of the oxygen content and was not detected with conventional XRD. ZrN phase is present, but when the oxygen content increases, the relative intensity of ZrN (111) peak decreases.

The patterns of samples $ZrN_{1.14}O_{0.14}$ and $ZrN_{0.95}O_{0.22}$ present broad and asymmetric peaks, with the last one significantly shifted to higher angles. The XRD pattern of sample $ZrN_{0.87}O_{0.30}$ presents a nearly symmetrical peak, with lower width and located almost in the position correspondent

Table 1
Composition and thickness of the films

Sample	Zr (at.%)	N (at.%)	O (at.%)	Thickness (μm)
$Zr(NO)_x$ ($x \ll 1$)	>80	[a]	[a]	9.6±0.4
$ZrN_{1.14}O_{0.14}$	44	50	6	2.3±0.2
$ZrN_{0.95}O_{0.22}$	46	44	10	3.0±0.2
$ZrN_{0.87}O_{0.30}$	46	40	14	3.0±0.2

[a] In sample $Zr(NO)_x$, the Zr content is dominant and determination of an accurate percentage of N and O was not possible.

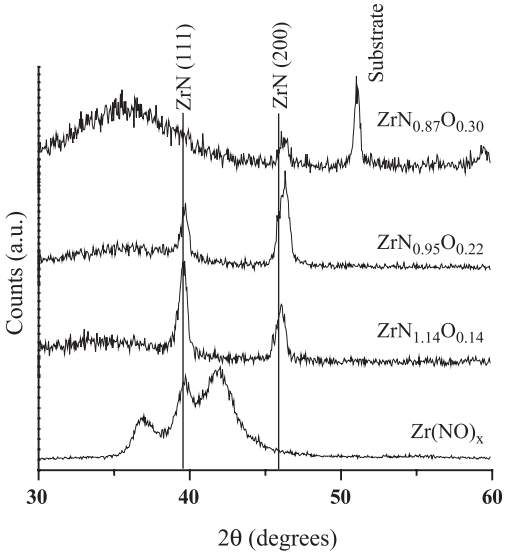

Fig. 1. GIXRD patterns of as-deposited ZrN_xO_y samples.

to the stress-free (200) ZrN position. What is the cause of this behaviour? In sample $ZrN_{1.14}O_{0.14}$, when the oxygen content is low (6 at.%), the insertion of O atoms in ZrN lattice might happen, probably in interstitial sites, leading to a broad and asymmetrical peak, in a state of nonuniform compressive microstress. The broad peaks would then be the result of the overlap of diffraction peaks corresponding to different lattice parameters. With higher O content (sample $ZrN_{0.95}O_{0.22}$), the asymmetric peak seems to be an overlap of two peaks (Fig. 3): one of them (A) less intense and located at a lower 2θ value, and the other (B) at a higher 2θ value when compared to the position of unconstrained ZrN (200) diffraction peak. Peak A should be assigned to ZrN (200) in a state of compressive microstress. Peak B is significantly more intense and is located at an angular position that cannot be

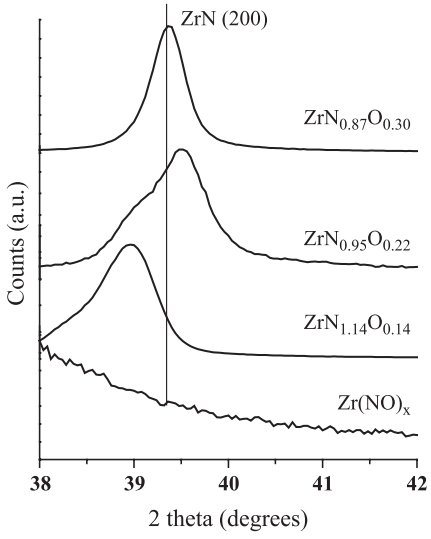

Fig. 2. Conventional XRD of as-deposited ZrN_xO_y samples around the angular position of peak ZrN (200) (the line indicates the unstressed position of the peak).

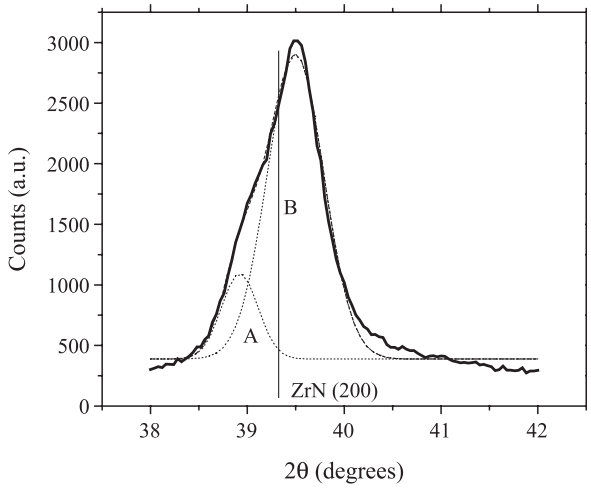

Fig. 3. Conventional XRD of as-deposited $ZrN_{0.95}O_{0.22}$ sample around the angular position of peak ZrN (200) and fitting with two Gaussian functions, evidencing ZrN phase (fit A) and Z–N–O phase (fit B). The line indicates the unstressed position of the ZrN (200) peak.

attributed to ZrO_2 or α-$ZrN_{0.28}$ phases. This probably means that some ZrN crystallites could be embedded in an amorphous Zr–N–O matrix, which would result in a nearly unstressed position of the (200) ZrN diffraction peak. Another possibility is the formation of a Zr–N oxygen-doped phase (noted as Zr–N–O phase), and the position of the correspondent stress-free peak should be located at a higher angular position when compared to that one correspondent of ZrN (200) diffraction peak. Anyway, it is clear that these findings are very difficult to index to any of the existing crystalline phases, composed of the three elements present in these films (Zr, O, and N); thus, the exact nature of the different crystalline phases revealed in this work needs subsequent analyses in order to clarify these doubts.

For the sample with higher O content (sample $ZrN_{0.87}O_{0.30}$), the nearly symmetrical peak is probably correspondent to the same effect of ZrN crystallites embedded in the amorphous phase, or to a dominant Zr–N–O phase in a state of compressive microstress. The thermal treatment in vacuum conditions will help to understand this behaviour and will be discussed in Section 3.3.2.

3.3. Structure evolution during heat treatment

XRD patterns show, as expected, that the heat treatment up to 900 °C causes an increase of the degree of crystallinity of the ceramic coatings. The significant structural changes are detected essentially at temperatures higher than 600 °C.

3.3.1. Heat treatment in controlled atmosphere

The diffraction peaks detected before thermal treatments remain after all the experiments carried out between 400 and 900 °C, but become sharper due to suppression of defects promoted by the annealing process, including the loss or autodiffusion of oxygen and/or nitrogen atoms from interstitial sites, inducing some possible stress relaxation. The development of new peaks from zirconium oxide phases appears at temperature of 600 °C or higher. The GIXRD patterns of the sample $Zr(NO)_x$, shown in Fig. 4, evidence this behaviour. This is due to the combination of different processes, where the stress relaxation induced by reduction of defects, including segregation of nitrogen and oxygen atoms originating from interstitial sites to grain boundaries, is certainly one of the most relevant. These stress relaxations will cause a decrease of disorder in crystallites (Zr, α-$ZrN_{0.28}$, and ZrN) and a rearrangement of Zr, O, and N atoms, or the development of monoclinic and tetragonal phases of zirconia (m-ZrO_2 and t-ZrO_2) and zirconium nitride (fcc phase) crystallites.

The GIXRD patterns of the remaining three samples reveal, as temperature increases, the appearance of t-ZrO_2 with detection of diffraction peaks corresponding to (011) and (112) planes. This effect is detected mainly above 600 °C and is caused by the organization of the zirconium oxide amorphous phase, existing at grain boundaries, forming tetragonal crystallites and is shown in Fig. 5 for the sample $ZrN_{0.95}O_{0.22}$. These GIXRD patterns reveal no significant changes in ZrN peaks.

3.3.2. Heat treatment in vacuum

The conventional $\theta/2\theta$ XRD patterns of these samples are more difficult to analyse because of the presence of peaks corresponding to the zirconium interlayer. Nevertheless, it is observed that peak width decreases and the angular position of the ZrN peaks shifts to higher values, which is an indication of the annealing of defects and some stress relaxation. This is clearly observed in Fig. 6 for sample $Zr(NO)_x$. The broad peak of the diffraction pattern of the as-deposited sample develops to a narrower and more intense peak corresponding to the XRD in planes (111) of ZrN. This may be interpreted as a possible segregation of interstitial atoms from ZrN lattice to grain boundaries. The

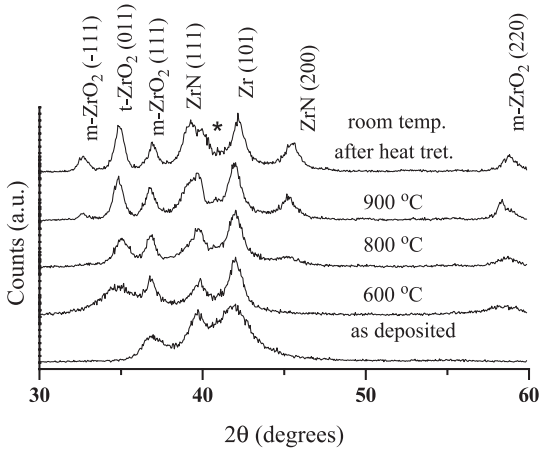

Fig. 4. GIXRD patterns of $Zr(NO)_x$ during heat treatment in controlled atmosphere conditions: m—monoclinic phase of zirconia; t—tetragonal phase of zirconia. *Peak corresponding to overlap of Zr (002), α-Zr(N) (002), and m-ZrO_2 (002).

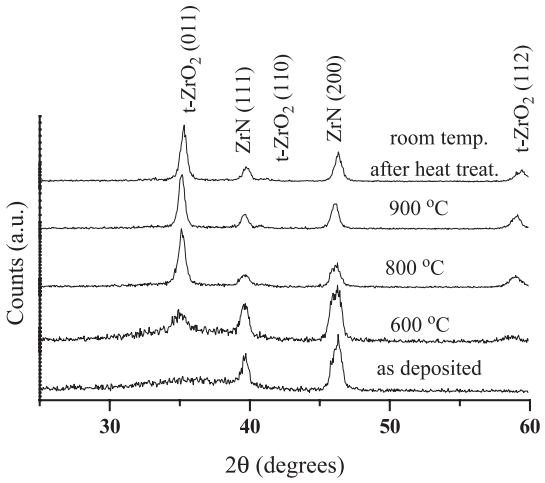

Fig. 5. GIXRD patterns of sample $ZrN_{0.95}O_{0.22}$, during heat treatment, in controlled atmosphere conditions.

XRD pattern of the as-deposited sample shows large bands around the angular position of Zr, and/or α-$ZrN_{0.28}$ (100) and (101) plane diffraction peaks. Anyway, the conventional $\theta/2\theta$ configuration does not allow distinguishing if these peaks correspond to the interlayer or ceramic coatings.

The XRD patterns of the remaining samples show that the relative intensity of Zr (002) peak from the interlayer strongly increases as the temperature of the thermal treatment rises, mainly when compared with ZrN peaks (Fig. 7a, sample $ZrN_{1.14}O_{0.14}$). This is maybe due to the increase of crystallinity in the interlayer. The intensity of ZrN peaks is increasing and reveals a state of compressive microstress, decreasing when temperature rises. The Zr planes, from the interlayer, are in a state of compressive microstress, but their interplanar distances increase (Fig. 7b) due to the lower thermal linear expansion coefficient of the zirconium. This behaviour is detected for all the samples.

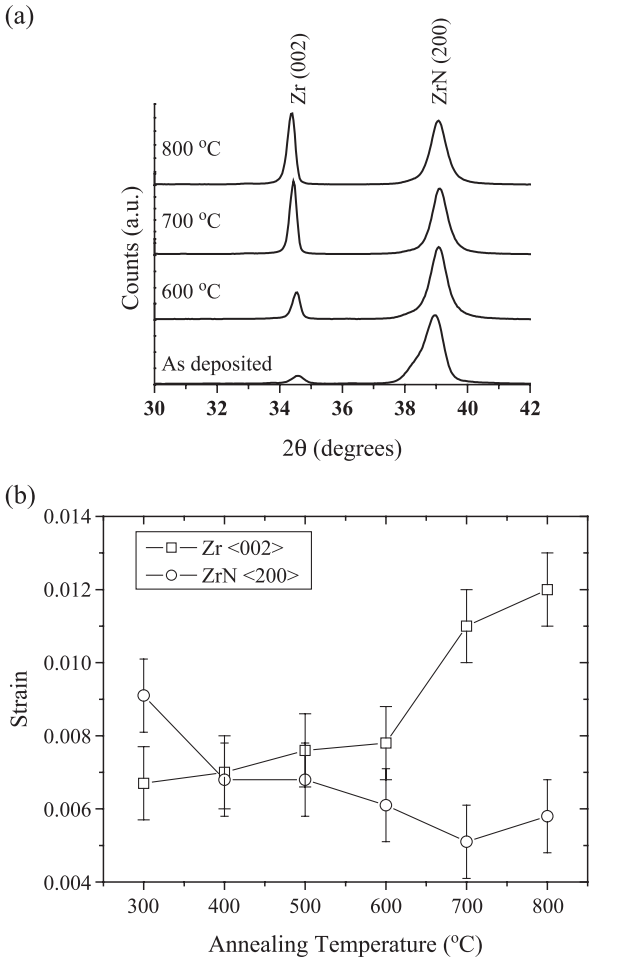

Fig. 7. Sample $ZrN_{1.14}O_{0.14}$. (a) Conventional XRD patterns after each annealing temperature in vacuum condition. (b) Strain in ZrN (measured in (200) planes) and Zr (measured in (002) planes) crystallites, as a function of temperature.

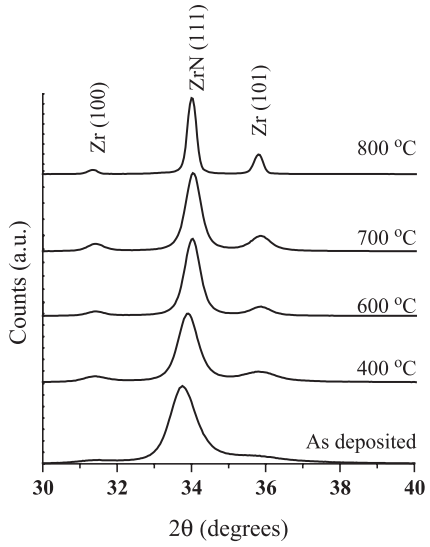

Fig. 6. Conventional XRD patterns of sample $Zr(NO)_x$ after each annealing temperature in vacuum conditions.

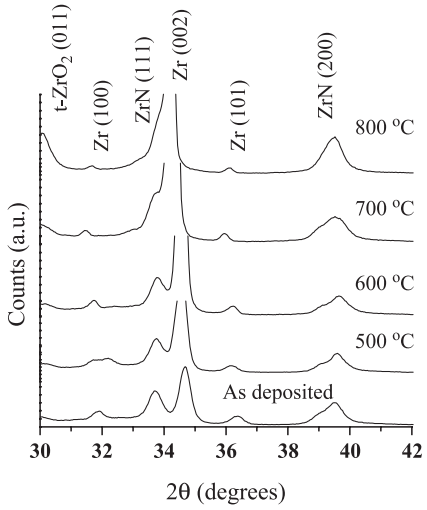

Fig. 8. Conventional XRD patterns of sample $ZrN_{0.95}O_{0.22}$ after each annealing temperature, in vacuum conditions.

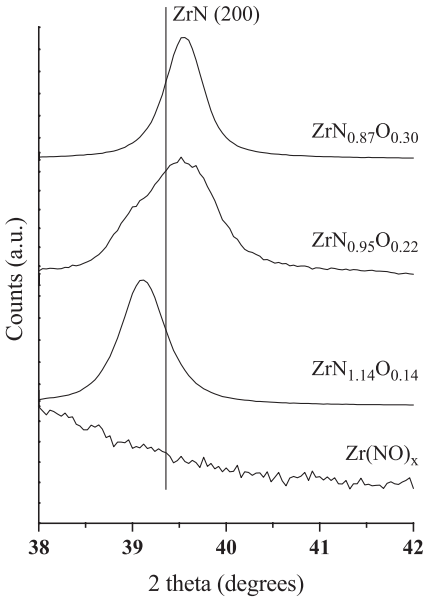

Fig. 9. Conventional XRD of ZrN_xO_y samples around the angular position of peak ZrN (200), after complete vacuum annealing process (the line indicates the unstressed position of the peak).

At 800 °C and for sample $ZrN_{0.95}O_{0.22}$ (Fig. 8), a strong increase in relative intensity of the peak corresponding to (011) planes of t-ZrO_2 is detected. This peak started to be evident at 700 °C and it seems that, at this temperature, there are good conditions for the formation of tetragonal zirconia crystallites.

It is interesting to verify again the XRD pattern of these samples around the angular position of ZrN (200) after the entire vacuum annealing process (Fig. 9). No significant change is detected for sample $Zr(NO)_x$, but the behaviour of the other three samples may help to understand their structure. The width of the peak of sample $ZrN_{1.14}O_{0.14}$ decreased, became nearly symmetrical, and shifted to higher angular positions. This behaviour is expected and is due to defect annealing and stress releases. Sample $ZrN_{0.95}O_{0.22}$ has a different behaviour. The overlap of two peaks before the annealing process was discussed in Section 3.2. For this sample, the annealing process provokes an expected shift to higher angles, but the asymmetry caused by the overlap of peaks A and B is maintained. It seems that both phases discussed previously (ZrN and Zr–N–O) remain after the annealing and both suffer a stress release process.

The heat treatment of sample $ZrN_{0.87}O_{0.30}$ causes a shift of the diffraction peaks to higher angles, maintaining its symmetry. This behaviour seems to confirm the dominant Zr–N–O phase in a process of stress relaxation.

4. Conclusions

Structural characterization of ZrN_xO_y thin films reveals a strong dependence of the observed behaviour on the film composition. The higher nitrogen partial pressure induces the formation of ZrN crystallites, but the presence of oxygen in reactive atmosphere leads to the formation of a zirconium oxide amorphous phase and induces nonuniform microstress in ZrN crystallites due to possible insertions of O atoms in crystalline lattice. For higher oxygen content in the films, the diffraction peaks seem to indicate a mixture of ZrN crystallites at different stress states and probably a new phase with oxygen incorporation (Zr–N–O phase).

When zirconium atomic content is higher than 80%, the heat treatment in controlled atmosphere reveals the annealing of defects and the formation of several phases, including m-ZrO_2 and t-ZrO_2. When the oxygen content of the films varies from 6 to 14 at.%, the GIXRD reveals the development of t-ZrO_2 phase at temperatures of 600 °C or higher.

The results obtained after vacuum annealing reveal the stress relaxation in crystallites detected after deposition. The analyses of conventional XRD data obtained after each annealing temperature seem to indicate the possible existence of a Zr–N–O phase for films with higher oxygen content (at 10 and 14 at.%).

Acknowledgements

The authors gratefully acknowledge the financial support of the FCT institution through project no. POCTI/CTM/38086/2001 cofinanced by the European Community Fund FEDER.

References

[1] L. Hultman, Vacuum 57 (2000) 1.
[2] S. Ventkartaraj, O. Kappertz, R. Jayavel, M. Wuttig, J. Appl. Phys. 92 (5) (2002) 2461.
[3] B. Zega, Surf. Coat. Technol. 39/40 (1989) 507.
[4] C. Mitterer, J. Komenda-Stallmaier, P. Losbichler, P. Schmolz, W.S.M. Werner, H. Stori, Vacuum 46 (1995) 1281.
[5] H.K. Pulker, Coatings on Glass, Thin Films Science and Technology, vol. 6, Elsevier, Amsterdam, 1984.
[6] N. Martin, O. Banakh, A.M.E. Santo, S. Springer, R. Sanjinés, J. Takadoum, F. Lévy, Appl. Surf. Sci. 185 (2001) 123.
[7] F. Fabreguette, L. Imhoff, M. Maglione, B. Domenichini, M.C.M. Lucas, P. Sibillot, S. Bourgeois, M. Saciolotti, Chem. Vap. Depos. 6 (3) (2000) 109.
[8] C. Rousselot, N. Martin, Surf. Coat. Technol. 142–144 (2001) 206.
[9] N. Martin, R. Sanjinés, J. Takadoum, F. Lévy, Surf. Coat. Technol. 142–144 (2001) 615.
[10] J.-M. Chappe, N. Martin, G. Terwagne, J. Lintymer, J. Gavoille, J. Takadoum, Thin Solid Films 440 (2003) 66.
[11] F. Vaz, P. Cerqueira, L. Rebouta, C. Nascimento, E. Alves, Ph. Goudeau, J.P. Rivière, Surf. Coat. Technol. 174–175 (2003) 197.
[12] F. Vaz, P. Cerqueira, L. Rebouta, S.M.C. Nascimento, E. Alves, Ph. Goudeau, J.P. Rivière, K. Pischow, J. de Rijk, Thin Solid Films 447–448 (2003) 449.
[13] S. Collard, H. Kupfer, W. Hoyer, G. Hecht, Vacuum 55 (1999) 1453.
[14] C.J. Rosa, W.C. Hagel, J. Electrochem. Soc. 115 (1968) 467.
[15] Hj. Matzke, V.V. Rondinella, in: D.L. Beke (Ed.), Diffusion in Carbides, Nitrides, Hydrides and Borides, Landolt-Börnstein Numerical Data and Functional Relationship in Science and Technology, vol. 33, Springer, Berlin, 1999, Chap. 5.
[16] L.R. Doolittle, Nucl. Instrum. Methods B9 (1985) 344.